Article

Combinatorial synthesis of oxysulfides in the lanthanum-bismuth-copper system

Mitsutaro Umehara, Lan Zhou, Joel A. Haber, Dan Guevarra, Kevin Kan, Paul F Newhouse, and John M. Gregoire

ACS Comb. Sci., **Just Accepted Manuscript** • Publication Date (Web): 30 Apr 2020

Combinatorial synthesis of oxysulfides in the lanthanum-bismuth-copper system

Mitsutaro Umehara, [a,b,†,§] *Lan Zhou,*[a,†] *Joel A. Haber,*[a] *Dan Guevarra,*[a] *Kevin Kan,*[a] *Paul F. Newhouse,*[a] *John M. Gregoire*[a,c,*]

[a] Joint Center for Artificial Photosynthesis, California Institute of Technology; Pasadena, California 91125, United States; [b] Future Mobility Research Department, Toyota Research Institute of North America, Ann Arbor, MI 48105, United States; [c] Division of Engineering and Applied Science, California Institute of Technology, Pasadena, CA 91125, United States

[†] These authors contributed equally

[§] Current address: Toyota Central Research and Development Laboratories, Inc., 41-1 Yokomichi, Nagakute, Aichi 480-1192, Japan

Corresponding Author

*gregoire@caltech.edu

Abstract:

Establishing synthesis methods for a target material comprises a grand challenge in materials research, which is compounded with use-inspired specifications on the format of the material. Solar photochemistry using thin film materials is a promising technology for which many complex materials are being proposed, and the present work describes application of combinatorial methods to explore the synthesis of predicted La-Bi-Cu oxysulfide photocathodes, in particular alloys of LaCuOS and BiCuOS. The variation in concentration of 3 cations and 2 anions in thin film materials, and crystallization thereof, is achieved by a combination of reactive sputtering and thermal processes including reactive annealing and rapid thermal processing. Composition and structural characterization establish composition-processing-structure relationships that highlight the breadth of processing conditions required for synthesis of LaCuOS and BiCuOS. The relative irreducibility of La oxides and limited diffusion indicate the need for high temperature processing, which conflicts with the temperature limits for mitigating evaporation of Bi and S. Collectively the results indicate that alloys of these phases will require reactive annealing protocols that are uniquely tailored to each composition, motivating advancement of dynamic processing capabilities to further automate discovery of synthesis routes.

Keywords: combinatorial synthesis, oxysulfide, thermal processing, solar fuels

TOC figure:

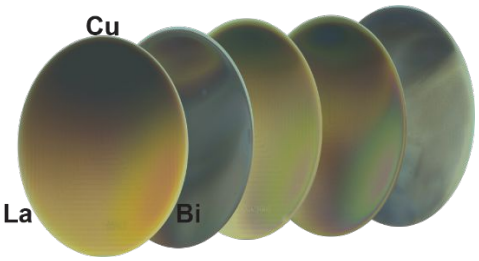

Introduction

Synthesis of solid state materials is a critical component of science and technology,[1-2] especially in the age of computer-accelerated design of materials with application-specific properties.[3] In solar photochemistry, mixed anion compounds have been proposed as promising materials for achieving the combination of chemical stability, visible light absorption, and charge carrier transport.[4] BiCuOS has recently been explored as a photocatalyst[5] and alloys of the form $La_{1-x}Bi_xCuOS$ have been predicted to enable band gap energy variation from 1.1 to 2.9 eV to provide chemistry-tuned utilization of the solar spectrum.[6] Cu-based oxides and oxychalcogenides comprise a promising class of transparent conductors,[7] and LaCuOS has been studied in this context.[7-10] This class of materials presents composition complexity for which combinatorial methods could accelerate materials exploration and understanding. Among the challenges in combinatorial library synthesis is anion stoichiometry control, for which deposition strategies have been developed, e.g. for nitrogen,[11] although due to the issues of introducing sulfur into thin film deposition systems, where a small but impactful vapor pressure of sulfur can persist for years, there is a strong preference to develop combinatorial synthesis techniques that introduce S via post-deposition processing. Sulfurization via thermal processing in a flowing H_2S atmosphere is a commonly employed technique[12] and is amenable to combinatorial experimentation by loading a composition library into a sufficiently large tube furnace. Since H_2S and its partial decomposition into H_2 can reduce (remove oxygen from) thin films, thermal processing protocols must be developed to establish sulfur and oxygen stoichiometries that enable formation of oxysulfide phases. In the present work we demonstrate combinatorial synthesis combined with x-ray fluorescence and x-ray diffraction mapping to accelerate the development of such processing conditions.

The composition-dependent kinetics and thermodynamics limit the design of thermal processing protocols to obtain the desired thin film composition and phase. Models for predicting synthesis protocols are being developed, for example via machine learning from the literature for solid state materials[13] and combining machine learning with human insights[14] and symbolic AI[15] for molecular synthesis. While these powerful approaches will undoubtedly be useful in specific settings, the proposed synthesis of thin film oxysulfide alloys is not amenable to synthesis design by such models at this time, due to the lack of relevant training data, both with respect to the La-Bi-Cu oxysulfide chemistry and with respect to the thin film format of complex oxysulfides. An outstanding challenge for machine learning across the physical sciences is to learn from partial information. In the present work, data related to synthesis, in order from least expensive (highest throughput) to most expensive (lowest throughput) includes metals and sulfur composition, XRD structural characterization, and oxygen concentration. The thousands of data points collected via combinatorial experimentation may be in the range of

applicability for some machine learning models, but the heterogeneity of the data and expert knowledge required to establish relationships among these different data sources, and to reason about known thermodynamics of related materials and which synthesis steps may be kinetically or thermodynamically limited, require future development of artificial intelligence for materials.[16] Consequently, the present work focuses on combinatorial experimentation techniques to explore synthesis conditions and establish processing-composition-structure relationships. Learning such trends across broad regions of composition space complement detailed characterization of an individual synthesis, which can also provide data for building synthesis prediction models.[2]

The oxysulfide compounds BiCuOS and LaCuOS have been synthesized by a number of methods due to their interesting properties and potential applications in thermoelectrics, p-type transparent conductive oxides, superconductivity, solar energy conversion, etc.[7] However, due to the significantly different physical and chemical properties of Bi and La compounds, the synthesis conditions reported to date differ significantly for the two target compounds. For example, the widely used ceramic method of mixing and heating elemental or binary compound precursor powders in a sealed ampule, requires a processing temperature of 350°C for the Bi compound,[17] and 750 to 900°C for the La compound.[9-10, 18] In calorimetry measurements, the BiCuOS compound decomposes by loss of S at 560°C, and segregation of small amounts of elemental Bi is observed at temperatures as low as 270°C.[19] In 2-step synthesis BiCuOS was annealed up to 500°C in sealed ampules to obtain good crystallinity, while LaCuOS was annealed at 800°C in sealed ampules.[20] Soft solution phase syntheses require significantly different conditions, due to the fundamentally different chemistry of Bi and La. Using a room temperature precipitation followed by high temperature H_2 reduction to produce LaCuOS requires a reduction temperature of 800 °C.[21] The BiCuOS is readily synthesized using hydrothermal methods at 250°C,[22] but this route cannot produce LaCuOS, due to the greater basicity of Lanthanum oxides stabilizing $La(OH)_3(aq)$ to temperatures in excess of 800 °C under hydrothermal conditions.[22] However, using solvothermal synthesis based on ethylenediamine (en), with precise control over the hydration level of the precursor compounds, enables synthesis of LaCuOS at 200°C.[10] It is not known if BiCuOS can be prepared under similar non-aqueous solvothermal conditions. LaCuOS has been prepared in thin film form via deposition of a multilayered La_2O_3 and Cu_2O thin film followed by sulfurization at 860°C in a sealed furnace with ca. 1 atm S vapor.[8] The present work uses a similar strategy of depositing precursor oxide thin films with subsequent sulfurization, using La-Bi-Cu composition libraries to combinatorially explore the synthesis space using flowing H_2S to incorporate S at lower processing temperatures.

Methods

Deposition

The La-Bi-Cu oxide composition libraries were synthesized by radio-frequency (RF) reactive co-sputtering in a custom-designed combinatorial sputtering system[23] followed by thermal processing. All the libraries were deposited at room temperature onto 100 mm-diameter XG glasses in a mixed atmosphere of O_2 (0.16 Pa) and Ar (0.64 Pa) using La, Bi, and Cu metal targets placed in magnetron sputtering cathodes located 120° apart with respect to the plane of the glass substrates, at a distance of 2.14 cm from substrate center, and tilted 15° toward the chamber center with respect to vertical. The deposition proceeded for 8 hours with the RF powers on La, Bi, and Cu sources set to be 67, 15, and 34 W, respectively, to obtain the desired composition spread.

Thermal processing

As-deposited La-Bi-Cu oxide libraries were sulfurized in a 4.5 inch quartz tube research furnace (PVI) using a mixture of 5% hydrogen sulfide (H_2S) in nitrogen (N_2), back-filled at room temperature to 10 Torr then held at a constant pressure with a total flow rate of 240 sccm over the course of the anneals. A fixed ramp rate of 15°C per minute was used for all tube furnace anneals, where soak temperatures ranged from 120°C to 500°C. Libraries were cooled at ca. 2.5°C per minute to 80°C before evacuating the 5% H_2S atmosphere and purging with N_2.

Vacuum annealing was performed in the same 4.5 inch quartz tube furnace as sulfurization. Prior to the anneal, residual gas (air) was nominally reduced to part per billion levels following three consecutive pump-purge cycles with N_2. A vacuum level of 30 mTorr was maintained through active pumping over the course of the 32 minutes ramp, 120 minutes hold at 500°C, and cooldown to 80°C before purging with N_2.

After sulfurization, select composition libraries were subjected to a series of rapid thermal anneals in flowing Ar to induce crystallization while mitigating changes to anion stoichiometry. A Modular Process RTP600S modified for top-down heating was used to carry out the anneals. Substrates were placed in the 9 L RTP chamber on a graphite susceptor, purged with high purity Ar at a flow rate of 10 lpm for 7 minutes to provide an inert annealing atmosphere, then heated with a 30 second ramp up to peak temperature in a lower flow rate of 4 lpm to avoid convective heat losses, followed by immediate cooling down in a flow rate 10 lpm. The RTP process limits significant in-film diffusion, and O, S anions loss from the films. The thermocouple measured the temperature of sample susceptor, so the actual thin films may have been heated to different temperatures due to composition-specific optical properties.

Characterization

The crystal structure of the films were determined by x-ray diffraction (XRD) measurements using a Bruker DISCOVER D8 diffractometer with Cu K_α radiation from a Bruker IμS source. The x-ray spot size was limited to a 2 mm length scale, over which the composition is constant to within approximately 1 at.%. The XRD images were collected by a two-dimensional VÅNTEC-500 detector and integrated into one-dimensional patterns using DIFFRAC.SUITE™ EVA software. The crystal structures present in each sample were identified by matching the XRD patterns with entries in the International Crystallography Diffraction Database (ICDD).

The bulk cation and anion S compositions in each library were determined by x-ray fluorescence (XRF) measurements using an EDAX Orbis Micro-XRF system with an x-ray beam approximately 2 mm in diameter. The sensitivity factor for each element was calibrated using commercial XRF calibration standards (MicromatterTM). The oxygen stoichiometry was not specifically controlled or measured in the sputtered composition libraries. We refer to the oxysulfide compositions as $La_xCu_yBi_{1-x-y}S_rO_z$, where x, y, and r (S-to-metal ratio) were determined by XRF.

The anion O and S composition mapping was measured with a FEI Nova NanoSEM 450 scanning electron microscope equipped with an energy dispersive x-ray spectroscopy (EDS) detector (Oxford Instruments X-Max 80 mm^2) using a low energy electron beam of 5 kV and working distance of 7 mm. The measurement conditions were confirmed to limit the sampling volume to within the thickness of the

thin film materials by the absence of elemental signals from substrate elements, e.g. Si. The software used for data acquisition and analysis was INCA.

Optical characterization was performed using a custom-built, on-the-fly High-throughput scanning spectroscopy instrument.[24] Briefly, the dual integrating sphere system measured both the fractional transmittance (T) and reflectance (R) at 1521 locations across the entire 100 mm glass substrate (measurement pitch = 2 mm) using illumination from a 200 W (Hg)Xe broadband source and spectrometers. The T and R signals were used to calculate the spectral absorption coefficient (α) up to a factor of film thickness (τ): $\alpha \times \tau = -\ln[T \times (1-R)-1]$. The molar absorption coefficient was calculated by making τ the molar thickness from the XRF-measured molar concentration of La, Cu and Bi.

Results and Discussion

The reactive annealing of metal oxides in H_2S can be regarded as a metathesis reaction in which the formation of metal sulfides is promoted by the generation of the thermodynamic sink H_2O as a byproduct, as shown in Equation (1), which is continuously removed in the flowing system:

$$M_2O_3 + Cu_2O + 2\ H_2S \rightarrow 2\ MCuOS + 2\ H_2O \qquad (1)$$

Thus, this process for producing metal sulfides is energetically favorable, even when starting from very stable metal oxides. The main limitation to this conversion process is the kinetics of reacting the relatively stable H_2S molecule and diffusion through the thin film; thus, relatively high reaction temperatures are often required. In the current reaction the desired goal is to replace ½ of the initial oxygen in the solid with sulfur, to produce a layered oxysulfide with alloying of La and Bi in the oxygen-containing layer. Because both of the unalloyed compounds, BiCuOS and LaCuOS, have been experimentally prepared as pure compounds by several synthetic methods, their energetic stability relative to lower order compounds has been empirically demonstrated. The *ab initio* assessment of $Bi_{1-x}RE_xCuOS$ (RE = La, Gd, Y, Lu) solid solutions shows appreciable stabilization of all alloy compositions for $Bi_{1-x}La_xCuOS$ relative to the unalloyed compositions,[6] supporting the feasibility of synthesizing a range of $Bi_{1-x}La_xCuOS$ alloy compositions.

The anticipated challenge to producing the alloyed 1:1 O:S composition is the significant divergence in reported reaction temperatures reported for BiCuOS and LaCuOS, as described above. Therefore, a range of sulfidation temperatures were employed to produce films with similar O:S ratios, typically followed by rapid thermal processing (RTP) to induce crystallization.

Starting from 4 La-Bi-Cu oxide composition libraries, which are similar in composition due to static deposition parameters (see Fig. S1), a series of thermal processing steps were applied, involving various combinations of annealing (i) in flowing 5% H_2S in N_2 in a tube furnace, (ii) RTP in Ar atmosphere, and (iii) annealing in 0.03 Torr vacuum after N_2-flush in a tube furnace. Processing by any of these 3 methods puts the library into a new state, which is annotated by an alphabetically increasing letter followed by an integer indicating the composition library. Table 1 enumerates the various library states for the 4 composition libraries with noted thermal processing histories.

Fig. 1 shows photographs of the 100 mm-diameter XG glass substrates with composition libraries in the as-deposited state (A1) and after a series of thermal processes in H_2S. The general trend of darkening with higher temperature processing is accompanied by subtle color changes at various combinations of

composition and thermal processing temperature. Fig. 2 shows XRF-based composition maps of the metals loading and sulfur-to-metal concentration at select states, where the La-Cu-Bi composition at each library location was measured for each of the states. Comparison of different states from the same library provides characterization of changes in sulfur stoichiometry, cation composition changes, and cation loss via evaporation due to the interim thermal process(es).

The RTP in Ar atmosphere is expected to be sufficiently short in duration to mitigate reactions between the bulk of the thin film and the atmosphere. This assumption was confirmed in our previous study of oxynitrides,[25-26] although we suspect that the near-surface will change S and/or O stoichiometry during RTP. While the limited extent of such composition changes has a small effect on XRF measured composition and negligible effect on measured XRD signal, for purposes of studying surface-sensitive properties, including photocatalysis, the beneficial or deleterious effects of heterogeneous surface layers must be evaluated. For the purposes of the present work, the S-to-metal from before and after RTP can be compared to ensure that no appreciable S loss occurred. In Fig. 2, states P4 and D1 share a common 4 hour H_2S processing, with P4 having an additional 411°C RTP in Ar. The similar S-to-metal values and composition trends support the assumption of no bulk composition changes during RTP.

Fig. 3 shows the series of XRD patterns starting with the H_2S processed thin film (state D1) where the metals composition $La_{0.09}Cu_{0.46}Bi_{0.45}$ corresponds to the lowest La concentration with approximately equal Cu:Bi. This is the cation composition closest to the target phase BiCuOS and is denoted by a black circle in the D1 plot in Fig. 2. Over the sequence of RTP at increasing temperatures, Cu-Bi sulfide phases are observed, and at the highest 2 temperatures there appears to be a small fraction of a Bi oxysulfide phase and Bi_2O_3. The S-to-metal of the starting material is lower than ideal by about a factor of 2, bringing into question whether an off-stoichiometry of S and/or O make thermodynamics unfavorable for BiCuOS or whether kinetic barriers favor formation of the observed competing phases. No evidence of LaCuOS was observed at the corresponding La-rich compositions, although in this case no other crystalline phases were observed, as shown in Fig. S2. Combinatorial XRD experiments revealed interesting phase behavior at cation composition $La_{0.30}Cu_{0.28}Bi_{0.42}$, which is denoted by a gray circle in the D1 plot in Fig. 2. The series of XRD patterns for this composition is shown in Fig. 4, where similar to Fig. 3 Cu_3BiS_3 is the first observed phase, i.e. after 320°C RTP in Ar. With RTP at 409°C and above, the target BiCuOS structure is observed and coexists with Bi_2O_3. Given the starting cation composition, the excess Bi compared to Cu is consistent with the segregation of Bi_2O_3, and segregation of a third of the Bi into this secondary phase would leave Bi:Cu:S in the correct stoichiometry for BiCuOS. Comparison to the results of Fig. 2 suggests that formation of BiCuOS structure requires that the pre-RTP film to have a Cu:S ratio close that of the formula unit, whereas the metal-to-metal and other metal-to-S values can be further from the respective formula unit value. For the $La_{0.30}Cu_{0.28}Bi_{0.42}$ sample, this leaves a sizable La concentration unexplained by the XRD interpretation. The possibility of La alloying into BiCuOS is discussed below, although given the lack of crystallization in the La-rich region, segregation of an x-ray amorphous La oxide phase in this film is a plausible explanation.

The observations from the series of thermal processes on this first composition library include (i) the need to explore higher temperature H_2S anneals for S incorporation into La-rich compositions (ii) the need for higher temperature and/or longer duration annealing to attempt crystallization of LaCuOS. The combination of irreducibility of La oxides as well as limited diffusion in La-rich compositions is consistent with prior hydrothermal and sealed ampule syntheses where 800°C and higher temperatures are typically used.[8, 20-21] To address (i), the second library was processed in H_2S at 200°C for 1 hour, resulting

in state L2 where S-to-metal was successfully increased for most of the La-Bi-Cu compositions (see Fig. 2). To address (ii), the library was subsequently annealed at 500°C for 3 hours, resulting in state M2 where nearly all Bi has evaporated from the film, as evidenced by the XRF compositions condensing onto the La-Cu binary line in Fig. 2. The vapor pressure of Bi over Bi metal is ca. 6 10^{-5} Torr, and while higher pressures have been observed over Bi_2S_3, the corresponding vapor was found to primarily S species.[27] The Bi pressure over the multi-metal, O and S-containing film is unknown, but using the nominal value of Bi metal, the ca. 1 μmol cm^{-2} loading of Bi could evaporate within 10 minutes at 500°C in the absence of a diffusion limitation within the thin film, which is the simplest explanation for the Bi loss during the 3 hour vacuum anneal.

Interestingly, the most La-rich compositions in state M2 prevent Bi evaporation at concentrations up to ca. 10% Bi, likely due to a combination of lowered Bi vapor pressure and diffusion-limited evaporation. XRD analysis identified the LaCuOS over a range of compositions starting with $La_{0.48}Cu_{0.50}Bi_{0.02}S_{0.43}$, which is close to the formula unit stoichiometry with a slight S deficiency, and extending to more La rich compositions. At La concentrations near 60%, the LaCuOS structure is observed with a range of Bi concentrations from 0.03 to 0.08, as indicated by the red oval in Fig. 2, and the XRD pattern of most Bi-rich sample shown in Figure 5. There is no evidence of alloying-based peak shifting, and no other phase is observed. The excess La is more substantial than the Bi, suggesting an x-ray amorphous La-Bi component to the film, although the possibility of Bi substitution onto the La site in the LaCuOS structure is discussed below.

Given the successful synthesis of LaCuOS but the undesirable loss of Bi, an additional synthesis was attempted on the third composition library, a single anneal in H_2S at 500°C for 1 hour, resulting in state N3. The film exhibited some Bi loss but not nearly to the extent of state M2, suggesting a lower Bi vapor pressure than in the vacuum anneal and/or lower Bi diffusion due to different composition and structure due to the different thermal history. This higher temperature H_2S process yielded higher S-to-metal in La-rich compositions but lower S-to-metal in Cu-rich compositions, likely due to the high partial pressure of S over CuS. Various sulfide phases were observed at Cu-rich and Bi-rich compositions, and the target LaCuOS phase was observed at a similar La-rich composition as that noted for state L2, as indicated by the red oval in Fig. 2 and XRD pattern in Fig. 5. The sharper XRD peaks suggest a larger domain size for the phase under this processing condition, although the XRD still has no sign of the excess La and Bi compared to the LaCuOS formula unit. Compared to previous syntheses of LaCuOS, the present work is unique in the relatively low temperatures required and demonstration of phase formation starting from a range of metal compositions, including the near-stoichiometric composition in state M2 and La-rich compositions in states M2 and N3.

Returning attention to the BiCuOS phase, the fourth library was processed using maximum temperatures based on state H1, which corresponds to the lowest RTP temperature at which the phase was observed. H_2S anneal at 160°C for 4 hours followed by 411°C RTP in Ar (state P4) yielded the BiCuOS structure near composition $La_{0.45}Cu_{0.29}Bi_{0.27}S_{0.28}$ (see red oval in Fig. 2), which has Bi:Cu:S in the formula unit stoichiometry, but once again there is a large concentration of La that appears to be x-ray amorphous in the XRD pattern of Fig. 5. To ascertain why the phase is not formed with lower La concentrations, the oxygen stoichiometry was characterized using EDS. Using a low beam energy of 5 kV to mitigate beam penetration through the thin film of interest, the S K and O K peaks were used to measure the O-to-S ratio across the composition library. The O loading in the thin film was then calculated from the S loading from XRF measurements, producing the O-to-S and O-to-metal ratios

shown in Fig. 6. Given the propagation of possible systematic errors in these calculations, the uncertainty in each value is approximately 20%, although the relative values that characterize the composition trends have uncertainty primarily from composition-dependent matrix effects, which are expected to be relatively small. The results show that the Bi:Cu = 1 region is O-poor compared to BiCuOS, which is consistent with the observation of primarily sulfide phases in Fig. 3. O concentration generally increases with La concentration, so the role of the excess La in successful synthesis of the BiCuOS structure may be avoidance of O loss during the reductive H_2S processing. The variation in O stoichiometry by a factor of 10 over the range of metals composition highlights the confluence of composition-dependent thermodynamics and kinetics, indicating that vastly different H_2S processing conditions would be required to obtain the desired O and S stoichiometries. Indeed this is a motivation for the sealed ampule-type syntheses described above and poses a challenge to accelerated experimentation efforts that are largely incompatible with sealed ampule syntheses.

Mapping of the spectral transmission and reflection provided characterization of composition-dependent spectral absorption for select libraries. To visualize trends in absorption for photon energies pertinent to solar photocatalysis, the average absorption coefficient from 2 to 2.5 eV was calculated for each composition sample. While absorption coefficients are typically reported as the attenuation coefficient per film thickness, we normalize by the metal molar density in the present work, as that value is provided by the XRF measurements (see Fig. 2) and this normalization facilitates visualization of how metal and sulfur concentrations impact absorption. The resulting composition plots of average molar absorption are shown in Fig. 7. Comparison to the S-to-metal values in Fig. 2 reveal a general increase in absorption with increased S concentration; the Pearson correlation coefficient between average molar absorption and S-to-metal for the set of all data points in Fig. 7 is 0.53. Average molar absorption is also somewhat correlated with Bi concentration with a coefficient value of 0.32. The data in Fig. 7 is consistent with LaCuOS being weakly absorbing, BiCuOS being moderately absorbing, and Bi and Bi-Cu sulfides being highly absorbing in the visible, demonstrating the wide range of optical absorption exhibited by the La-Bi-Cu-O-S composition system, although per the effort to obtain the target oxysulfide phases, the optical absorption is only useful for photocatalysis given chemical stability and photovoltaic-like energy conversion.

The optical data show increased absorption with La-to-Bi composition gradients, consistent with the proposed band gap tuning in $La_{1-x}Bi_xCuOS$, but there remains no structural evidence of such alloying in these composition libraries. At the same time, there is no structural evidence for phase segregation of LaCuOS and BiCuOS as these phases are never found to coexist due to incompatible H_2S and thermal processing conditions. The synthesis incompatibilities likely arise from differences in sulfurization thermodynamics and both S and O diffusion kinetics, as suggested by the variation in melting temperatures of the binary metal oxides and sulfides (2307°C for La_2O_3, 2100-2150°C for La_2S_3, 825°C for Bi_2O_3, 685°C for decomposition of Bi_2S_3, 1326°C for CuO, 500°C for CuS). These differences limit the ability to obtain the same degree of sulfidation over a broad range of metal stoichiometries. Ideally, enough S incorporation would occur at each composition to be stoichiometric with the Cu; however, under conditions which achieve appropriate S incorporation in Bi-rich compositions, little S incorporation occurs in La-rich regions. Following RTP processing, the La-rich components likely remain as amorphous oxides. In contrast, under processing conditions suitable for S incorporation into the La-rich compositions, nearly complete sulfidation and partial decomposition of the Bi-rich regions occurs, leading to Bi depletion. Thus, it is not possible to simultaneously synthesize both LaCuOS and BiCuOS in

the same library; moreover, due to the divergent sulfidation and crystallization requirements of La compounds and Bi compounds, we observed no conclusive La-Bi substitutional alloying into either parent compound.

In the MCuOS structures, M is coordinated to 4 O on one side and 4 S on the other. The Shannon ionic radii of Bi^{+3} and La^{+3} in 8-fold coordination are 131 and 130 pm, respectively. With this small difference in radius, it may be possible to alloy substantially into each MCuOS end member phase without noticeable changes in lattice constants in our XRD experiments. Lattice constant modulation must occur at some alloy concentration considering the difference in lattice constants of the end member phases. Even though each phase was obtained in a composition with excess of the target alloying element (LaCuOS with excess Bi and BiCuOS with excess La), each XRD pattern matches to a single end member phase with no substantial peak shifting that would indicate alloying-based modulation of lattice constants. Thus there is no evidence of substantial alloying under the range of synthesis conditions explored herein, although the similar ionic radii inhibit establishment of the maximum solubility into each end member phase.

As noted above, S incorporation by reactive annealing is required when a dedicated deposition system for S-containing materials is not available. The dedication of such a system creates opportunities for controlling stoichiometry in thin films to avoid the diffusion and evaporation limitations of thermal processing. For LaCuOS, this has been demonstrated by sputtering from custom-made sintered targets of the desired stoichiometry,[7] although co-sputtering from metal oxide and metal sulfide targets is an alternate strategy. Additional axes for composition control can be achieved by introducing other S sources, which could include H_2S as a sputtering gas, which requires detailed safety considerations, especially if O_2 is included as an O source. Alternatively, S plasma sources provide an opportunity for S stoichiometry control and tailored S concentration gradients, and initial results indicate that this route is effective for vacuum deposition of metal oxysulfides and could enable a various combinatorial syntheses.[28]

To explore mixed-anion materials via thermal processing, the present work provides strong motivation for the development of combinatorial reactive annealing techniques that can capitalize on parallel synthesis, such as co-sputter composition libraries, and enable independent thermal processing of different compositions. Combinatorial heating strategies using discrete[29] and continuous[30] temperature gradients have been demonstrated, and laser spike annealing[31] comprises a strategy for spatially resolved heating, providing independent temperature history of different compositions while additionally enabling thermal processing at time scales much smaller than RTP. Coupling such local heating techniques with control of the atmosphere above the heated thin film, and ultimately with XRD or other structural characterization for rapid feedback, would greatly accelerate development of synthesis protocols for generating thin films of complex materials, especially in mixed-anion composition spaces. High throughput XRF and XRD characterization of composition libraries can couple nicely with such serial-annealing techniques by providing rapid characterization of the processing landscape to seed design of serial processing conditions.

Acknowledgements

This study is based upon work performed by the Joint Center for Artificial Photosynthesis, a DOE Energy Innovation Hub, supported through the Office of Science of the U.S. Department of Energy (Award No. DE-SC0004993).

Competing Interests: The Authors declare no Competing Financial or Non-Financial Interests.

Supporting Information Available:

Table of relevant crystal structures and additional figures with composition, XRD and plate photographs.

References

1. *Basic Research Needs for Synthesis Science for Energy Relevant Technology*; Washington, DC, 2016.
2. Soderholm, L.; Mitchell, J. F., Perspective: Toward "synthesis by design": Exploring atomic correlations during inorganic materials synthesis. *APL Materials* **2016,** *4* (5), 053212.
3. Alberi, K.; Nardelli, M. B.; Zakutayev, A.; Mitas, L.; Curtarolo, S.; Jain, A.; Fornari, M.; Marzari, N.; Takeuchi, I.; Green, M. L.; Kanatzidis, M.; Toney, M. F.; Butenko, S.; Meredig, B.; Lany, S.; Kattner, U.; Davydov, A.; Toberer, E. S.; Stevanovic, V.; Walsh, A.; Park, N.-G.; Aspuru-Guzik, A.; Tabor, D. P.; Nelson, J.; Murphy, J.; Setlur, A.; Gregoire, J.; Li, H.; Xiao, R.; Ludwig, A.; Martin, L. W.; Rappe, A. M.; Wei, S.-H.; Perkins, J., The 2019 materials by design roadmap. *Journal of Physics D: Applied Physics* **2018,** *52* (1), 013001.
4. Maeda, K.; Domen, K., New non-oxide photocatalysts designed for overall water splitting under visible light. *J Phys Chem C* **2007,** *111* (22), 7851-7861.
5. Li, Y.; Zhu, J., Facile synthesis of BiCuOS for photocatalytic application. *Materials Letters* **2019,** *253*, 331-334.
6. Lardhi, S.; Curutchet, A.; Cavallo, L.; Moussab, H.; Le Bahers, T., Ab initio assessment of Bi1-xRExCuOS (RE = La, Gd, Y, Lu) solid solutions as a semiconductor for photochemical water splitting. *Physical Chemistry Chemical Physics* **2017,** *19* (19), 12321-12330.
7. Zhang, N.; Sun, J.; Gong, H., Transparent p-Type Semiconductors: Copper-Based Oxides and Oxychalcogenides. *Coatings* **2019,** *9* (2), 137.
8. Zhang, N.; Shi, D.; Liu, X.; Annadi, A.; Tang, B.; Huang, T. J.; Gong, H., High performance p-type transparent LaCuOS thin film fabricated through a hydrogen-free method. *Applied Materials Today* **2018,** *13*, 15-23.
9. Zhang, N.; Gong, H., P-type transparent LaCuOS semiconductor synthesized via a novel two-step solid state reaction and sulfurization process. *Ceramics International* **2017,** *43* (8), 6295-6302.
10. Doussier-Brochard, C.; Chavillon, B.; Cario, L.; Jobic, S., Synthesis of p-Type Transparent LaOCuS Nanoparticles via Soft Chemistry. *Inorganic Chemistry* **2010,** *49* (7), 3074-3076.
11. Han, Y.; Matthews, B.; Roberts, D.; Talley, K. R.; Bauers, S. R.; Perkins, C.; Zhang, Q.; Zakutayev, A., Combinatorial Nitrogen Gradients in Sputtered Thin Films. *ACS Combinatorial Science* **2018,** *20* (7), 436-442.
12. Gerein, N. J.; Haber, J. A., Synthesis of Cu3BiS3 Thin Films by Heating Metal and Metal Sulfide Precursor Films under Hydrogen Sulfide. *Chemistry of Materials* **2006,** *18* (26), 6289-6296.
13. Kim, E.; Huang, K.; Saunders, A.; McCallum, A.; Ceder, G.; Olivetti, E., Materials Synthesis Insights from Scientific Literature via Text Extraction and Machine Learning. *Chem Mater* **2017,** *29* (21), 9436-9444.
14. Badowski, T.; Gajewska, E. P.; Molga, K.; Grzybowski, B. A., Synergy Between Expert and Machine-Learning Approaches Allows for Improved Retrosynthetic Planning. *Angewandte Chemie International Edition* **2020,** *59* (2), 725-730.

15. Segler, M. H. S.; Preuss, M.; Waller, M. P., Planning chemical syntheses with deep neural networks and symbolic AI. *Nature* **2018,** *555* (7698), 604-610.
16. Gomes, C. P.; Selman, B.; Gregoire, J. M., Artificial intelligence for materials discovery. *MRS Bulletin* **2019,** *44* (7), 538-544.
17. Berthebaud, D.; Guilmeau, E.; Lebedev, O. I.; Maignan, A.; Gamon, J.; Barboux, P., The BiCu1−xOS oxysulfide: Copper deficiency and electronic properties. *Journal of Solid State Chemistry* **2016,** *237*, 292-299.
18. Nakachi, Y.; Ueda, K., Single crystal growth of LaCuOS by the flux method. *Journal of Crystal Growth* **2008,** *311* (1), 114-117.
19. Berardan, D.; Li, J.; Amzallag, E.; Mitra, S.; Sui, J.; Cai, W.; Dragoe, N., Structure and Transport Properties of the BiCuSeO-BiCuSO Solid Solution. *Materials* **2015,** *8* (3), 1043-1058.
20. Hiramatsu, H.; Yanagi, H.; Kamiya, T.; Ueda, K.; Hirano, M.; Hosono, H., Crystal Structures, Optoelectronic Properties, and Electronic Structures of Layered Oxychalcogenides MCuOCh (M = Bi, La; Ch = S, Se, Te): Effects of Electronic Configurations of M3+ Ions. *Chemistry of Materials* **2008,** *20* (1), 326-334.
21. Lian, J.; Li, N.; Wang, H.; Su, Y.; Zhang, G.; Liu, F., Synthesis of LaCuOS nanopowder by a novel precipitation combined with reduction route. *Ceramics International* **2016,** *42* (9), 11473-11477.
22. Sheets, W. C.; Stampler, E. S.; Kabbour, H.; Bertoni, M. I.; Cario, L.; Mason, T. O.; Marks, T. J.; Poeppelmeier, K. R., Facile Synthesis of BiCuOS by Hydrothermal Methods. *Inorganic Chemistry* **2007,** *46* (25), 10741-10748.
23. Suram, S. K.; Zhou, L.; Becerra-Stasiewicz, N.; Kan, K.; Jones, R. J. R.; Kendrick, B. M.; Gregoire, J. M., Combinatorial thin film composition mapping using three dimensional deposition profiles. *Review of Scientific Instruments* **2015,** *86* (3), 033904-033904.
24. Mitrovic, S.; Cornell, E. W.; Marcin, M. R.; Jones, R. J.; Newhouse, P. F.; Suram, S. K.; Jin, J.; Gregoire, J. M., High-throughput on-the-fly scanning ultraviolet-visible dual-sphere spectrometer. *Rev. Sci. Instrum.* **2015,** *86* (1), 013904.
25. Zhou, L.; Suram, S. K.; Becerra-Stasiewicz, N.; Mitrovic, S.; Kan, K., Combining reactive sputtering and rapid thermal processing for synthesis and discovery of metal oxynitrides. *J. Mater. Res.* **2015,** *30* (19), 2928-2933.
26. Suram, S. K.; Fackler, S. W.; Zhou, L.; N'Diaye, A. T.; Drisdell, W. S.; Yano, J.; Gregoire, J. M., Combinatorial Discovery of Lanthanum–Tantalum Oxynitride Solar Light Absorbers with Dilute Nitrogen for Solar Fuel Applications. *ACS Combinatorial Science* **2017**.
27. Piacente, V.; Gianfreda, V. D.; Bardi, G., Vapour pressure of solid Bi2S3. *The Journal of Chemical Thermodynamics* **1983,** *15* (1), 7-14.
28. Ford, J. C. Development of Earth Abundant Materials for Solar

Energy Conversion Using Combinatorial Experimentation. University of Colorado, Boulder, CO, 2015.
29. Stein, H.; Naujoks, D.; Grochla, D.; Khare, C.; Gutkowski, R.; Grützke, S.; Schuhmann, W.; Ludwig, A., A structure zone diagram obtained by simultaneous deposition on a novel step heater: A case study for Cu2O thin films. *physica status solidi (a)* **2015,** *212* (12), 2798-2804.
30. Siol, S.; Dhakal, T. P.; Gudavalli, G. S.; Rajbhandari, P. P.; DeHart, C.; Baranowski, L. L.; Zakutayev, A., Combinatorial Reactive Sputtering of In2S3 as an Alternative Contact Layer for Thin Film Solar Cells. *ACS Applied Materials & Interfaces* **2016**.
31. Bell, R. T.; Jacobs, A. G.; Sorg, V. C.; Jung, B.; Hill, M. O.; Treml, B. E.; Thompson, M. O., Lateral Temperature-Gradient Method for High-Throughput Characterization of Material Processing by Millisecond Laser Annealing. *ACS Combinatorial Science* **2016,** *18* (9), 548-558.

Table 1: Application of various thermal processings to 4 composition libraries (A1 to A4, sputter deposited La-Bi-Cu in 0.16 Pa O_2) results in a series of composition library states represented by their history of thermal processing. The state label includes an alphabetically increasing letter followed by an integer indicating the composition library. For example, library 2 was in state A2 after deposition, L2 after its first thermal processing, and M2 after its second thermal processing. The noted phases are often observed at different compositions for different states, as detailed below.

State name	Soak in 5% flowing H_2S		Soak in vacuum		RTP in Ar	Notable phases from XRD
	Temp. (°C)	Time (h)	Temp. (°C)	Time (h)	Peak Temp. (°C)	
A1-A4						
B1	120	1				
C1	160	1				
D1	160	3				
E1					320	Cu_3BiS_3
F1					344	Cu_3BiS_3
G1					375	Cu_3BiS_3
H1					409	BiCuOS + Cu_3BiS_3
I1					442	BiCuOS + Bi_2O_3
J1					460	BiCuOS + Bi_2O_3
K1					495	BiCuOS + Bi_2O_3
L2	200	1				
M2			500	3		LaCuOS
N3	500	1				LaCuOS
O4	160	4				
P4					411	CuBiOS

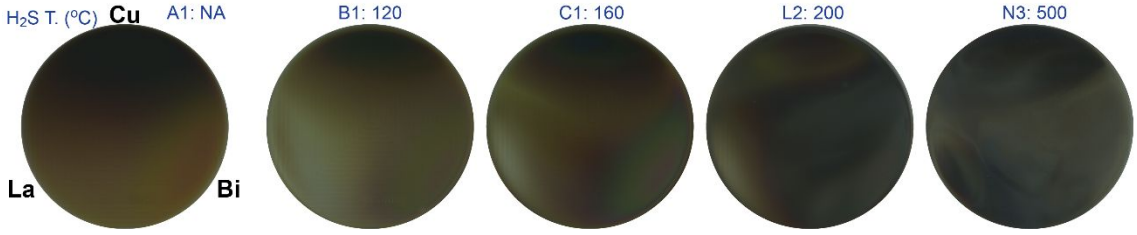

Fig. 1: Photographs of La-Bi-Cu composition libraries acquired in reflectance geometry in a photography box with diffuse reflecting walls and white light illumination. The as-deposited oxide library (A1) includes element labels corresponding to the respective arrangement of the deposition sources. The sequence of anneals in H_2S at increasing maximum temperature reveal complex, composition-dependent of optical properties. The library states are further defined in Table 1. The rectangular pattern of gray lines, particularly visible in the La-rich regions of B1, C1, and L2, are from the substrate holder and indicated optical transparency of the thin film.

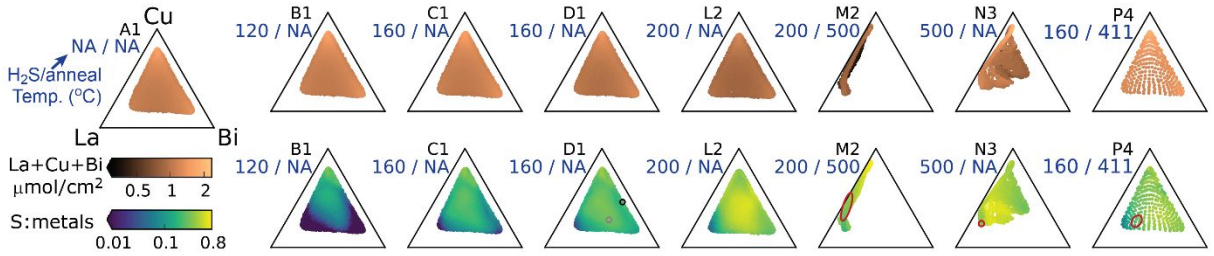

Fig. 2: XRF measurement of the La, Cu, Bi, and S molar densities provide La-Bi-Cu composition plots of the total metals loading (top) and S-to-metal ration (bottom), each plotted in log-scale false color as indicated at lower-left. The ternary composition plot labels for state A1 apply to all triangle plots. Below each library state label (see Table 1), the maximum temperatures from thermal processing in H_2S and subsequent RTP or vacuum annealing are provided. The black, gray and red annotations in the D1, M2, N3 and P4 plots are discussed below.

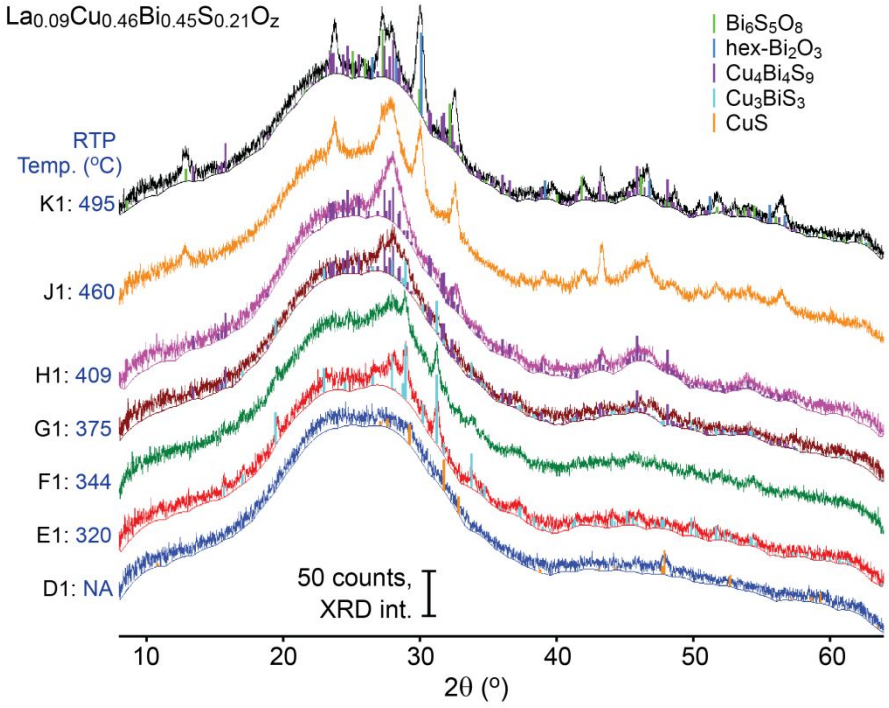

Fig. 3: Series of XRD patterns corresponding to increasing RTP temperatures, starting with the H_2S annealed state D1, whose XRF metals composition is $La_{0.09}Cu_{0.46}Bi_{0.45}$ with a sulfur-to-metal ratio of 0.21. The upper-right legend corresponds to the ICDD peak patterns, which are detailed further in Table S1.

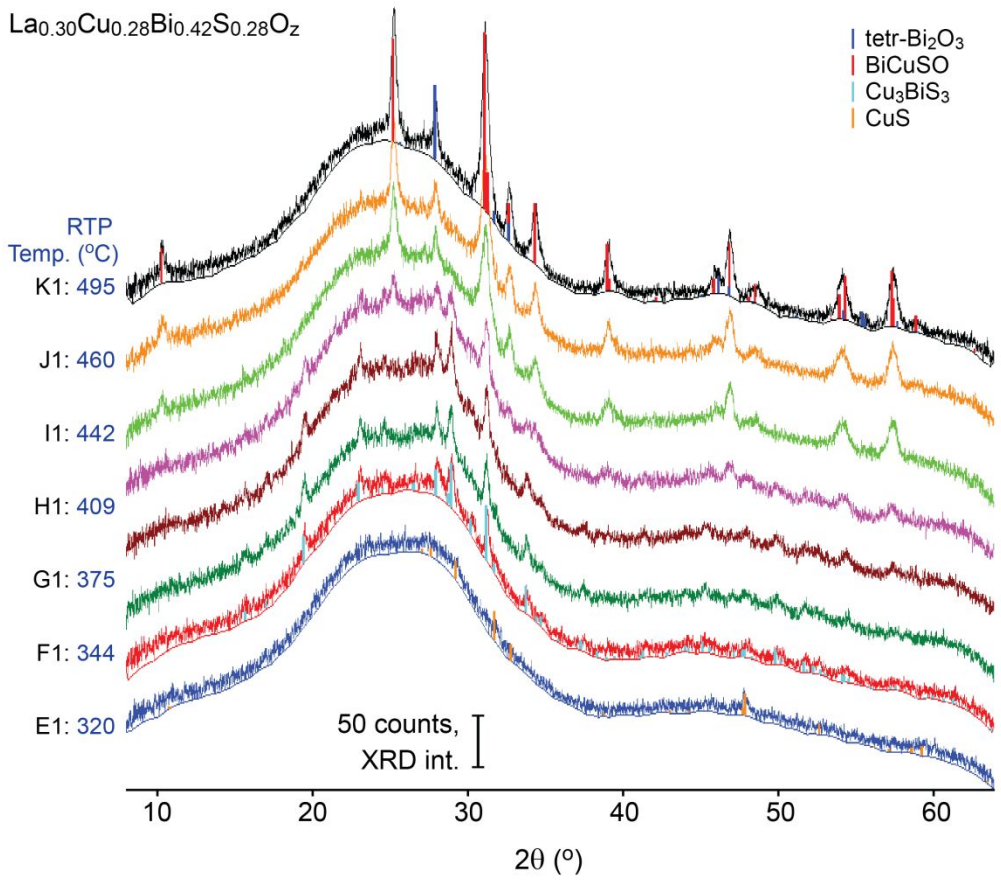

Fig. 4: Series of XRD patterns corresponding to increasing RTP temperatures, starting with the H_2S annealed state D1, whose XRF metals composition is $La_{0.30}Cu_{0.28}Bi_{0.42}$ with a sulfur-to-metal ratio of 0.28. The upper-right legend corresponds to the ICDD peak patterns, which are detailed further in Table S1.

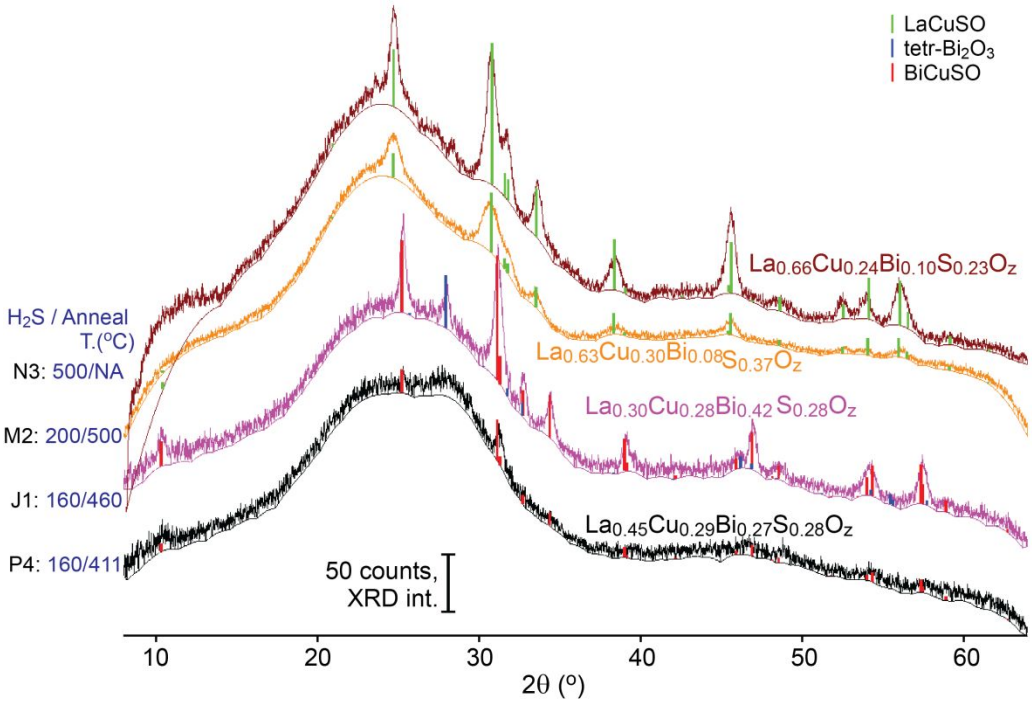

Fig. 5: Series of XRD patterns for 4 different library states and compositions where the target LaCuOS and BiCuOS phases were observed. With each library state label (see Table 1), the maximum temperature from thermal processing in H_2S and subsequent RTP or vacuum annealing are provided, and the XRF composition is noted for each pattern. While the target phase is the primary phase for each state, minor phases with insufficient signal for conclusive detection may also be present. The upper-right legend corresponds to the ICDD peak patterns, which are detailed further in Table S1.

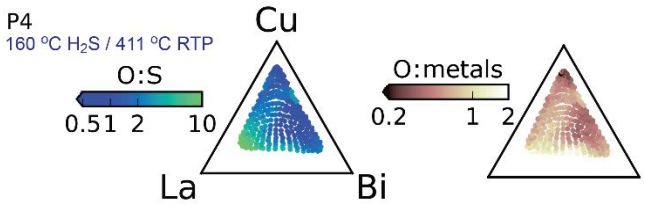

Fig. 6: For state P4, the XRF data of Fig. 2 combined with EDX measurements of the O-to-S ratio (left) are used to calculate the O-to-metals ratio (right). Both plots use a log-scale false color plot, as noted.

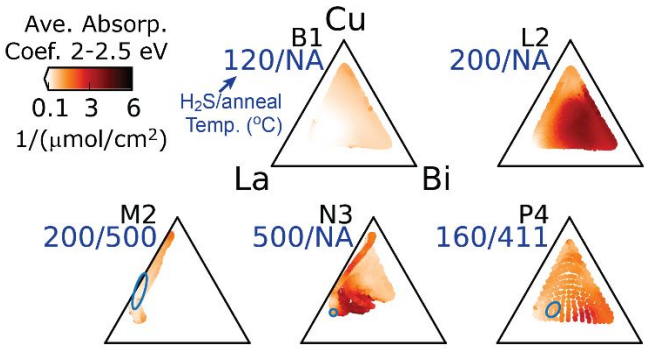

Fig. 7: The average molar absorption coefficient for 5 states (see Table 1), where the maximum temperatures from thermal processing in H_2S and subsequent RTP or vacuum annealing are noted. The molar absorption coefficient is calculated as the ratio of the unitless absorption coefficient and the molar concentration of metals (see Fig. 2). The LaCuOS and BiCuOS phase regions noted in red in Fig. 2 are noted in blue here.